Journal of the Physical Society of Japan
Vol. 69, No. 6, June, 2000, pp. 1757–1763

Spin-Orbit Interaction in Carbon Nanotubes

Tsuneya ANDO

Institute for Solid State Physics, University of Tokyo
7–22–1 Roppongi, Minato-ku, Tokyo 106-8666

(Received November 29, 1999)

An effective-mass Hamiltonian is derived for carbon nanotubes in the presence of a weak spin-orbit interaction. The spin-orbit interaction gives rise to terms corresponding to a kind of a spin-Zeeman energy due to magnetic fields in the circumference and axis direction. As a result spin scattering is induced even by spin-independent scatterers.

KEYWORDS: graphite, carbon nanotube, effective-mass theory, spin relaxation, spin-orbit interaction

§1. Introduction

A carbon nanotube (CN) is composed of concentric tubes of rolled two-dimensional (2D) graphite sheets, on which hexagons are arranged in a helical fashion about the axis.[1)] The diameter of a multi-wall nanotube ranges from 20 to 300 Å and that of a single-wall nanotube lies between 7 and 16 Å.[2,3)] The maximum length of nanotubes exceeds 1μm. Since the first discovery quite a number of studies have been reported on their electronic properties because of their unique topological structures. The purpose of this paper is to study effects of a spin-orbit interaction in a $\boldsymbol{k}\cdot\boldsymbol{p}$ scheme.

Various calculations have been performed to predict energy bands.[4−12)] Their characteristic properties are all reproduced quite well in a $\boldsymbol{k}\cdot\boldsymbol{p}$ method.[13,14)] The $\boldsymbol{k}\cdot\boldsymbol{p}$ scheme is quite powerful in the study of effects of external fields such as magnetic and electric fields and of transport properties. In fact, it has been successful in the study of magnetic properties including the Aharonov-Bohm effect on the band gap,[15)] optical absorption spectra,[16,17)] and lattice instabilities in the presence and absence of a magnetic field.[18−20)] It has played an important role also in predicting unique transport properties for scatterers with long[21,22)] and short-range scatterers[23)] and for phonon scattering,[24)] and those of CN junctions.[25−27)]

In this paper an effective $\boldsymbol{k}\cdot\boldsymbol{p}$ Hamiltonian is derived by explicitly including a weak spin-orbit interaction present in carbon $2p$ orbitals. It is shown that the spin-orbit interaction gives rise to terms corresponding to effective magnetic fields in the circumference and axis directions.

§2. Spin-Orbit Interaction

Figure 1 gives a schematic illustration of atomic $2p$ orbitals in a carbon nanotube. The orbital in the direction normal to the cylinder surface is denoted as $|z_j)$, that in the direction parallel to the axis as $|y_j)$, and that in the circumference direction as $|x_j)$. We choose the coordinate system (X, Y, Z) as shown in Fig. 1. The angle θ_j denotes the direction of the $|z_j)$ orbital measured from the Z direction.

In a two-dimensional graphite, the carbon $|x_j)$ and $|y_j)$ orbitals lying in the graphite plane having energy $\varepsilon_{2p}^{\sigma}$ are lower in energy than the $|z_j)$ orbital directed in the direction perpendicular to the plane having energy ε_{2p}^{π} because of crystal field effect, i.e., due to the attractive potential of neighboring carbon atoms. Define $\varepsilon_{\pi\sigma} = \varepsilon_{2p}^{\pi} - \varepsilon_{2p}^{\sigma} > 0$.

The spin-orbit interaction is given by

$$\mathcal{H}_{\rm so} = \frac{\hbar}{4m^2c^2}(\vec{\nabla}V\times\boldsymbol{p})\cdot\vec{\sigma}, \tag{2.1}$$

where $V(\boldsymbol{r})$ is the atomic potential, m is the free-electron mass, c is the light velocity, $\boldsymbol{p}$ is the momentum operator, and $\vec{\sigma}$ is Pauli's spin matrix. Because the spin-orbit interaction in carbon atoms is known to be small, we shall consider its effect to the lowest order.

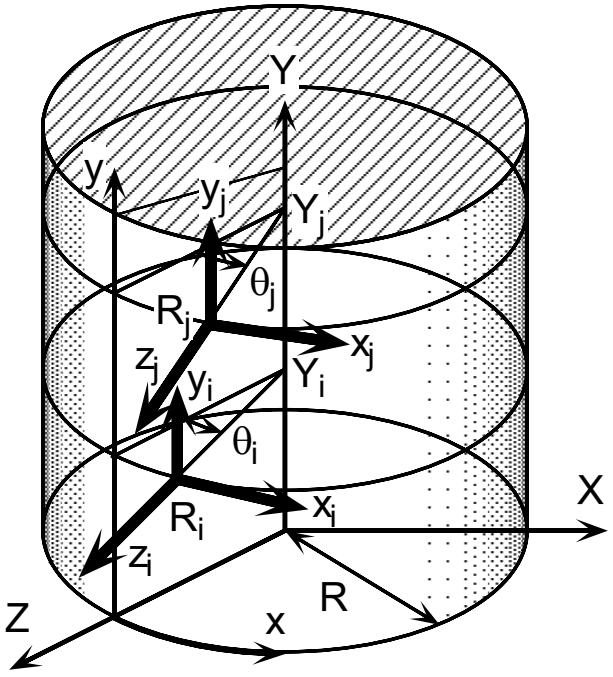

Fig. 1 A schematic illustration of $2p$ orbitals in carbon nanotubes and the coordinate system chosen in the text. The $2p$ orbitals localized at $\boldsymbol{r}_j$ are denoted as x_j, y_j, and z_j. The x axis is chosen in the circumference direction, the y axis in the axis direction, and z in the direction normal to the cylinder surface. The three-dimensional coordinates are given by (X, Y, Z).

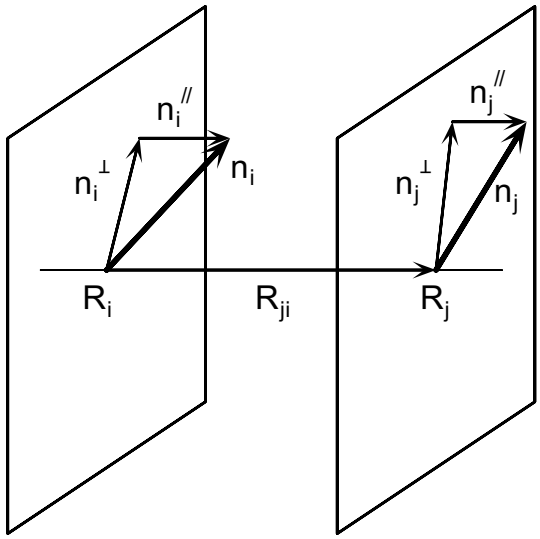

Fig. 2 A schematic illustration of two orbitals localized at $\boldsymbol{r}_j$ and $\boldsymbol{r}_i$. The unit vectors are given by $\boldsymbol{n}_j$ and $\boldsymbol{n}_i$.

Let $|\theta_j)$ and $|\bar{\theta}_j)$ be the eigen function of $\boldsymbol{n}(\theta_j)\cdot\vec{\sigma}$ with eigenvalue $+1$ and -1, respectively, where $\boldsymbol{n}(\theta_j)$ is the unit vector in the z_j direction defined by

$$\boldsymbol{n}(\theta_j) = (\sin\theta_j, 0, \cos\theta_j). \tag{2.2}$$

Then, in the lowest order perturbation theory, the wavefunction $|z_j\,\theta_j\rangle$ in the presence of a spin-orbit interaction is given by

$$\begin{aligned}|z_j\,\theta_j\rangle \approx |z_j\,\theta_j) &+ |x_j\,\bar{\theta}_j)\frac{(x_j\bar{\theta}_j|\mathcal{H}_{\rm so}|z_j\theta_j)}{\varepsilon_{\pi\sigma}}\\ &+ |y_j\,\bar{\theta}_j)\frac{(y_j\bar{\theta}_j|\mathcal{H}_{\rm so}|z_j\theta_j)}{\varepsilon_{\pi\sigma}},\end{aligned} \tag{2.3}$$

where $|z_j\theta_j)$, etc. denote states in the absence of a spin-orbit interaction. We have

$$\begin{aligned}(x_j\,\bar{\theta}_j|\mathcal{H}_{\rm so}|z_j\,\theta_j) &= -\frac{1}{3}\Delta,\\ (y_j\,\bar{\theta}_j|\mathcal{H}_{\rm so}|z_j\,\theta_j) &= -\frac{\mathrm{i}}{3}\Delta,\end{aligned} \tag{2.4}$$

with

$$\Delta = \mathrm{i}\frac{3\hbar}{4m^2c^2}\Big(x_j\Big|\frac{\partial V}{\partial x}p_y - \frac{\partial V}{\partial y}p_x\Big|y_j\Big). \tag{2.5}$$

Therefore, we have

$$|z_j\,\theta_j\rangle \approx |z_j\,\theta_j) - \delta|x_j + \mathrm{i}y_j\,\bar{\theta}_j), \tag{2.6}$$

with

$$\delta = \frac{1}{3}\frac{\Delta}{\varepsilon_{\pi\sigma}}. \tag{2.7}$$

Similarly, we have

$$|z_j\,\bar{\theta}_j\rangle \approx |z_j\,\bar{\theta}_j) + \delta|x_j - \mathrm{i}y_j\,\theta_j). \tag{2.8}$$

Let $|\uparrow)$ and $|\downarrow)$ be the spin function for up and down states in the Z direction, respectively. Then, we have

$$\begin{aligned}|\theta_j) &= +\cos\frac{\theta_j}{2}\,|\uparrow) + \sin\frac{\theta_j}{2}\,|\downarrow),\\ |\bar{\theta}_j) &= -\sin\frac{\theta_j}{2}\,|\uparrow) + \cos\frac{\theta_j}{2}\,|\downarrow),\end{aligned} \tag{2.9}$$

or

$$\begin{aligned}|z_j\uparrow\rangle &= \cos\frac{\theta_j}{2}\,|z_j\,\theta_j\rangle - \sin\frac{\theta_j}{2}\,|z_j\,\bar{\theta}_j\rangle,\\ |z_j\downarrow\rangle &= \sin\frac{\theta_j}{2}\,|z_j\,\theta_j\rangle + \cos\frac{\theta_j}{2}\,|z_j\,\bar{\theta}_j\rangle.\end{aligned} \tag{2.10}$$

Therefore, we have

$$\begin{aligned}|z_j\uparrow\rangle &= |z_j\uparrow) + \mathrm{i}\delta\sin\theta_j\,|y\uparrow) - \delta\big(|x_j\downarrow) + \mathrm{i}\cos\theta_j\,|y_j\downarrow)\big),\\ |z_j\downarrow\rangle &= |z_j\downarrow) - \mathrm{i}\delta\sin\theta_j\,|y\downarrow) + \delta\big(|x_j\uparrow) - \mathrm{i}\cos\theta_j\,|y_j\uparrow)\big).\end{aligned} \tag{2.11}$$

The same result can be obtained with the use of $\sigma_{xj} = \sigma_X\cos\theta_j - \sigma_Z\sin\theta_j$, $\sigma_{yj} = \sigma_y = \sigma_Y$, and $\sigma_{zj} = \sigma_X\sin\theta_j + \sigma_Z\cos\theta_j$, where $(\sigma_{xj}, \sigma_{yj}, \sigma_{zj})$ is the spin matrix in the coordinate system (x_j, y_j, z_j) and $(\sigma_X, \sigma_Y, \sigma_Z)$ is that in (X, Y, Z).

Consider the transfer integral for orbits ϕ_i localized at $\boldsymbol{R}_i$ and ϕ_j localized at $\boldsymbol{R}_j$, where $\phi = x$, y, or z. Let $\boldsymbol{n}(\phi_j)$ be a unit vector in the direction of the orbital ϕ_j. Then, we have

$$(\phi_i|V|\phi_j) = \big(\boldsymbol{n}(\phi_i)^{\parallel}, \boldsymbol{n}(\phi_j)^{\parallel}\big)V_{pp}^{\sigma} + \big(\boldsymbol{n}(\phi_i)^{\perp}, \boldsymbol{n}(\phi_j)^{\perp}\big)V_{pp}^{\pi}, \tag{2.12}$$

where V_{pp}^{σ} and V_{pp}^{π} are the transfer integral for σ and π orbitals, respectively, in a flat 2D graphite, $\boldsymbol{n}(\phi_j)^{\parallel}$ is the projection of $\boldsymbol{n}(\phi_j)$ onto the vector $\boldsymbol{R}_{ji} = \boldsymbol{R}_j - \boldsymbol{R}_i$, and $\boldsymbol{n}(\phi_j)^{\perp}$ is the projection onto a plane perpendicular to $\boldsymbol{R}_{ji}$, as shown in Fig. 2. We have

$$\boldsymbol{n}(\phi_j)^{\parallel} = \frac{\big(\boldsymbol{R}_{ji}, \boldsymbol{n}(\phi_j)\big)}{(\boldsymbol{R}_{ji}, \boldsymbol{R}_{ji})}\boldsymbol{R}_{ji}, \tag{2.13}$$

and

$$\boldsymbol{n}(\phi_j)^{\perp} = \boldsymbol{n}(\phi_j) - \frac{\big(\boldsymbol{R}_{ji}, \boldsymbol{n}(\phi_j)\big)}{(\boldsymbol{R}_{ji}, \boldsymbol{R}_{ji})}\boldsymbol{R}_{ji}. \tag{2.14}$$

Consequently, we have

$$\begin{aligned}(\phi_i|V|\phi_j) = &\big(\boldsymbol{n}(\phi_i), \boldsymbol{n}(\phi_j)\big)V_{pp}^{\pi}\\ &+ \frac{\big(\boldsymbol{n}(\phi_i), \boldsymbol{R}_{ji}\big)\big(\boldsymbol{n}(\phi_j), \boldsymbol{R}_{ji}\big)}{(\boldsymbol{R}_{ji}, \boldsymbol{R}_{ji})}(V_{pp}^{\sigma} - V_{pp}^{\pi}).\end{aligned} \tag{2.15}$$

The transfer integral for a spin-flip process is given by

$$\begin{aligned}\langle z_i\uparrow|V|z_j\downarrow\rangle \approx \delta\big[&(z_i|V|x_j) - (x_i|V|z_j)\\ &- \mathrm{i}\big(\cos\theta_j(z_i|V|y_j) - \cos\theta_i(y_i|V|z_j)\big)\big].\end{aligned} \tag{2.16}$$

First, we consider

$$\begin{aligned}(z_i|V|x_j) = &\big(\boldsymbol{n}(z_i), \boldsymbol{n}(x_j)\big)V_{pp}^{\pi}\\ &+ \frac{\big(\boldsymbol{n}(z_i), \boldsymbol{R}_{ji}\big)\big(\boldsymbol{n}(x_j), \boldsymbol{R}_{ji}\big)}{\big(\boldsymbol{R}_{ji}, \boldsymbol{R}_{ji}\big)}(V_{pp}^{\sigma} - V_{pp}^{\pi}).\end{aligned} \tag{2.17}$$

Explicitly, we have

$$\begin{aligned}\big(\boldsymbol{n}(z_i), \boldsymbol{n}(x_j)\big) &= \sin(\theta_i - \theta_j),\\ \big(\boldsymbol{n}(z_i), \boldsymbol{R}_{ji}\big) &= R\big[\cos(\theta_i - \theta_j) - 1\big],\\ \big(\boldsymbol{n}(x_j), \boldsymbol{R}_{ji}\big) &= -R\sin(\theta_i - \theta_j),\end{aligned} \tag{2.18}$$

where R is the diameter of CN and $(\boldsymbol{R}_{ji}, \boldsymbol{R}_{ji}) = (1/3)a^2$ for nearest neighbor pairs with a being the lattice con-

stant. Therefore, we have

$$(z_i|V|x_j) = V_{pp}^{\pi}\sin(\theta_i-\theta_j) + (V_{pp}^{\sigma}-V_{pp}^{\pi})\frac{3R^2}{a^2}\sin(\theta_i-\theta_j)[1-\cos(\theta_i-\theta_j)]. \tag{2.19}$$

Similarly, $(x_i|V|z_j)=-(z_i|V|x_j)$.

Next, we consider

$$(z_i|V|y_j) = \big(\boldsymbol{n}(z_i),\boldsymbol{n}(y_j)\big)V_{pp}^{\pi} + \frac{\big(\boldsymbol{n}(z_i),\boldsymbol{R}_{ji}\big)\big(\boldsymbol{n}(y_j),\boldsymbol{R}_{ji}\big)}{\big(\boldsymbol{R}_{ji},\boldsymbol{R}_{ji}\big)}(V_{pp}^{\sigma}-V_{pp}^{\pi}), \tag{2.20}$$

for which

$$\begin{aligned}&\big(\boldsymbol{n}(z_i),\boldsymbol{n}(y_j)\big)=0,\\ &\big(\boldsymbol{n}(z_i),\boldsymbol{R}_{ji}\big)=R\big[\cos(\theta_i-\theta_j)-1\big],\\ &\big(\boldsymbol{n}(y_j),\boldsymbol{R}_{ji}\big)=Y_{ji},\end{aligned} \tag{2.21}$$

with $Y_{ji}=Y_j-Y_i$. This gives

$$(y_i|V|z_j) = -(V_{pp}^{\sigma}-V_{pp}^{\pi})\frac{3RY_{ij}}{a^2}[1-\cos(\theta_i-\theta_j)]. \tag{2.22}$$

Similarly, $(z_i|V|y_j) = -(y_i|V|z_j)$. Therefore, the final result is given by

$$\begin{aligned}\langle z_i\uparrow|V|z_j\downarrow\rangle &= \delta\Big(+2V_{pp}^{\pi}\sin(\theta_i-\theta_j)\\ &+2(V_{pp}^{\sigma}-V_{pp}^{\pi})\frac{3R^2}{a^2}\sin(\theta_i-\theta_j)[1-\cos(\theta_i-\theta_j)]\\ &-\mathrm{i}(V_{pp}^{\sigma}-V_{pp}^{\pi})(\cos\theta_i+\cos\theta_j)\frac{3RY_{ij}}{a^2}[1-\cos(\theta_i-\theta_j)]\Big).\end{aligned} \tag{2.23}$$

In a completely similar manner,

$$\begin{aligned}\langle z_i\downarrow|V|z_j\uparrow\rangle &= \delta\Big(-2V_{pp}^{\pi}\sin(\theta_i-\theta_j)\\ &-2(V_{pp}^{\sigma}-V_{pp}^{\pi})\frac{3R^2}{a^2}\sin(\theta_i-\theta_j)[1-\cos(\theta_i-\theta_j)]\\ &-\mathrm{i}(V_{pp}^{\sigma}-V_{pp}^{\pi})(\cos\theta_i+\cos\theta_j)\frac{3RY_{ij}}{a^2}[1-\cos(\theta_i-\theta_j)]\Big).\end{aligned} \tag{2.24}$$

For a non-spin-flip matrix element, we have

$$\langle z_i\uparrow|V|z_j\uparrow\rangle \approx (z_i|V|z_j) - \mathrm{i}\delta\big(\sin\theta_i(y_i|V|z_j)-\sin\theta_j(z_i|V|y_j)\big), \tag{2.25}$$

which gives

$$\begin{aligned}\langle z_i\uparrow|V|z_j\uparrow\rangle &= V_{pp}^{\pi}\cos(\theta_i-\theta_j)\\ &-(V_{pp}^{\sigma}-V_{pp}^{\pi})\frac{3R^2}{a^2}[1-\cos(\theta_i-\theta_j)]^2\\ &+\mathrm{i}\delta\,(V_{pp}^{\sigma}-V_{pp}^{\pi})(\sin\theta_i+\sin\theta_j)\frac{3RY_{ij}}{a^2}[1-\cos(\theta_i-\theta_j)].\end{aligned} \tag{2.26}$$

Similarly,

$$\begin{aligned}\langle z_i\downarrow|V|z_j\downarrow\rangle &= V_{pp}^{\pi}\cos(\theta_i-\theta_j)\\ &-(V_{pp}^{\sigma}-V_{pp}^{\pi})\frac{3R^2}{a^2}[1-\cos(\theta_i-\theta_j)]^2\\ &-\mathrm{i}\delta\,(V_{pp}^{\sigma}-V_{pp}^{\pi})(\sin\theta_i+\sin\theta_j)\frac{3RY_{ij}}{a^2}[1-\cos(\theta_i-\theta_j)].\end{aligned} \tag{2.27}$$

First, we shall completely neglect terms of the order $(a/R)^2$, which are spin independent and given by

$$\begin{aligned}\langle z_i\sigma|V|z_j\sigma\rangle' &= V_{pp}^{\pi}[\cos(\theta_i-\theta_j)-1]\\ &-(V_{pp}^{\sigma}-V_{pp}^{\pi})\frac{3R^2}{a^2}[1-\cos(\theta_i-\theta_j)]^2.\end{aligned} \tag{2.28}$$

Effects of these terms will be discussed in §5. Then, we have

$$\begin{aligned}\langle z_i\uparrow|V|z_j\uparrow\rangle &= V_{pp}^{\pi}\\ &+\mathrm{i}\delta\,(V_{pp}^{\sigma}-V_{pp}^{\pi})(\sin\theta_i+\sin\theta_j)\frac{3RY_{ij}}{a^2}[1-\cos(\theta_i-\theta_j)].\end{aligned} \tag{2.29}$$

and

$$\begin{aligned}\langle z_i\downarrow|V|z_j\downarrow\rangle &= V_{pp}^{\pi}\\ &-\mathrm{i}\delta\,(V_{pp}^{\sigma}-V_{pp}^{\pi})(\sin\theta_i+\sin\theta_j)\frac{3RY_{ij}}{a^2}[1-\cos(\theta_i-\theta_j)].\end{aligned} \tag{2.30}$$

§3. Effective-Mass Equation

The lattice structure of a 2D graphite is shown in Fig. 3 together with the first Brillouin zone. A unit cell contains two carbon atoms denoted as A and B. In a 2D graphite, two bands having approximately a linear dispersion cross the Fermi level (chosen at $\varepsilon=0$) at K and K' points of the first Brillouin Zone. The wave vectors of the K and K' points are given by $\boldsymbol{K}=(2\pi/a)(1/3,1/\sqrt{3})$ and $\boldsymbol{K}'=(2\pi/a)(2/3,0)$.

For states in the vicinity of the Fermi level $\varepsilon=0$ of the 2D graphite, we assume that the total wavefunction is written as

$$\begin{aligned}\psi_{A\sigma}(\boldsymbol{R}) &= \exp(\mathrm{i}\boldsymbol{K}\cdot\boldsymbol{R})F_{A\sigma}^{K}(\boldsymbol{R})+\mathrm{e}^{\mathrm{i}\eta}\exp(\mathrm{i}\boldsymbol{K}'\cdot\boldsymbol{R})F_{A\sigma}^{K'}(\boldsymbol{R}),\\ \psi_{B\sigma}(\boldsymbol{R}) &= -\omega\mathrm{e}^{\mathrm{i}\eta}\exp(\mathrm{i}\boldsymbol{K}\cdot\boldsymbol{R})F_{B\sigma}^{K}(\boldsymbol{R})\\ &\quad+\exp(\mathrm{i}\boldsymbol{K}'\cdot\boldsymbol{R})F_{B\sigma}^{K'}(\boldsymbol{R}),\end{aligned} \tag{3.1}$$

in terms of the slowly-varying envelope functions $F_{A\sigma}^{K}$, $F_{B\sigma}^{K}$, $F_{A\sigma}^{K'}$, and $F_{B\sigma}^{K'}$, with η being the chiral angle between the chiral vector $\boldsymbol{L}=n_a\boldsymbol{a}+n_b\boldsymbol{b}$ and the x' axis fixed on the graphite plane, where n_a and n_b are integers, and $\boldsymbol{a}$ and $\boldsymbol{b}$ ($|\boldsymbol{a}|=|\boldsymbol{b}|=a$) are primitive translation vectors, as shown in Fig. 3(a).

In the nearest-neighbor tight-binding approximation, the equation of motion for an up-spin electron at a carbon A site is given by

$$\varepsilon\psi_{A\uparrow}(\boldsymbol{R}_A) = \sum_{\boldsymbol{R}_B}\Big[V(\boldsymbol{R}_A\uparrow;\boldsymbol{R}_B\uparrow)\psi_{B\uparrow}(\boldsymbol{R}_B) +V(\boldsymbol{R}_A\uparrow;\boldsymbol{R}_B\downarrow)\psi_{B\downarrow}(\boldsymbol{R}_B)\Big], \tag{3.2}$$

with

$$\begin{aligned}V(\boldsymbol{R}_A\uparrow;\boldsymbol{R}_B\uparrow) &= V_{\pi}\\ &+2\mathrm{i}\delta\,(V_{pp}^{\sigma}-V_{pp}^{\pi})\sin\theta(\boldsymbol{R})\frac{3R}{2a^2}(\boldsymbol{R}_{AB}\cdot\boldsymbol{t})\Big(\frac{\boldsymbol{R}_{AB}\cdot\boldsymbol{l}}{R}\Big)^2,\\ V(\boldsymbol{R}_A\uparrow;\boldsymbol{R}_B\downarrow) &= 2\delta\Big[V_{pp}^{\pi}\frac{\boldsymbol{R}_{AB}\cdot\boldsymbol{l}}{R}\\ &+(V_{pp}^{\sigma}-V_{pp}^{\pi})\frac{3R^2}{2a^2}\Big(\frac{\boldsymbol{R}_{AB}\cdot\boldsymbol{l}}{R}\Big)^3\\ &-\mathrm{i}(V_{pp}^{\sigma}-V_{pp}^{\pi})\cos\theta(\boldsymbol{R})\frac{3R}{2a^2}(\boldsymbol{R}_{AB}\cdot\boldsymbol{t})\Big(\frac{\boldsymbol{R}_{AB}\cdot\boldsymbol{l}}{R}\Big)^2\Big],\end{aligned} \tag{3.3}$$

where terms of the order $(a/R)^0$ and $(a/R)^1$ have been

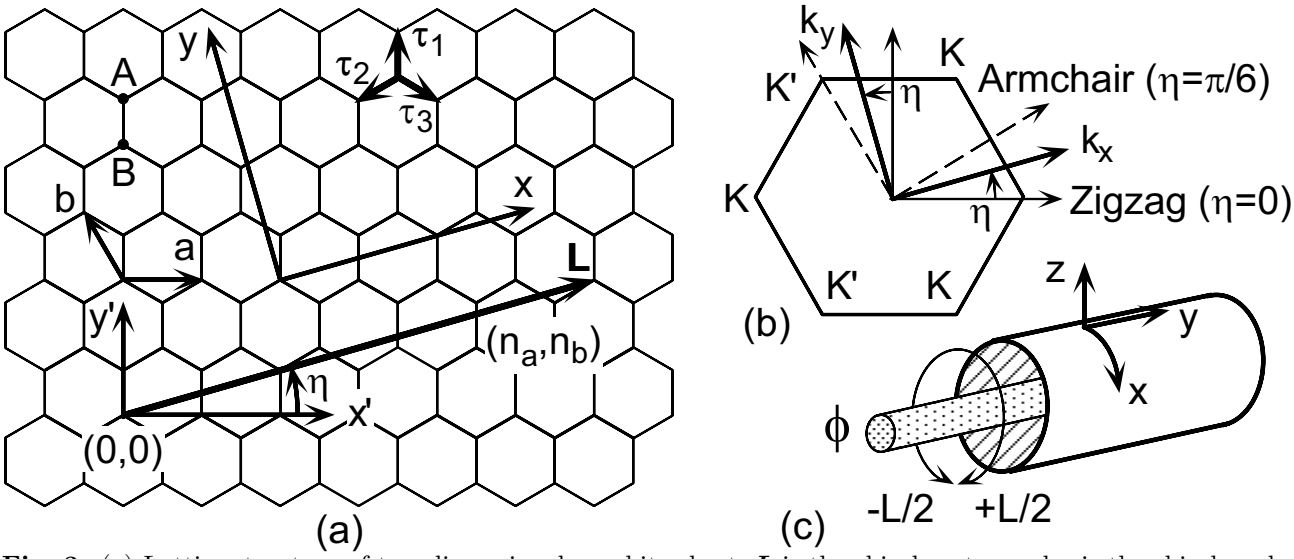

Fig. 3 (a) Lattice structure of two-dimensional graphite sheet, $\boldsymbol{L}$ is the chiral vector and η is the chiral angle. The coordinates (x', y') are fixed onto the graphite sheet and (x, y) are chosen in such a way that x is along the circumference of a nanotube and y is along the axis. (b) The first Brillouin zone and K and K' points. (c) The coordinates for a nanotube in the presence of a magnetic flux ϕ.

retained,

$$\theta(\boldsymbol{R}) = \frac{1}{2}[\theta(\boldsymbol{R}_A) + \theta(\boldsymbol{R}_B)] \approx \theta[(\boldsymbol{R}_A + \boldsymbol{R}_B)/2], \quad (3.4)$$

$\boldsymbol{R}_{AB} = \boldsymbol{R}_A - \boldsymbol{R}_B = \vec{\tau}_l$ $(l = 1, 2, 3)$ denotes a vector connecting neighboring A and B atoms as shown in Fig. 3(a), and $\boldsymbol{l} = (\cos\eta, \sin\eta)$ and $\boldsymbol{t} = (-\sin\eta, \cos\eta)$ are a unit vector in the circumference and axis direction, respectively.

The effective-mass equation in the presence of a spin-orbit interaction can be derived from the above tight-binding equation in a manner completely similar to that in previous papers.[14,20,21] First, we substitute eq. (3.1) into eq. (3.2) and use

$$\begin{aligned}
&\sum_l \mathrm{e}^{-\mathrm{i}\boldsymbol{K}\cdot\vec{\tau}_l} \begin{pmatrix} \tau_l^x & \tau_l^y \end{pmatrix} = \frac{\sqrt{3}}{2}\omega^{-1} a \begin{pmatrix} +\mathrm{i} & +1 \end{pmatrix}, \\
&\sum_l \mathrm{e}^{-\mathrm{i}\boldsymbol{K}'\cdot\vec{\tau}_l} \begin{pmatrix} \tau_l^x & \tau_l^y \end{pmatrix} = \frac{\sqrt{3}}{2} a \begin{pmatrix} -\mathrm{i} & +1 \end{pmatrix},
\end{aligned} \quad (3.5)$$

and

$$\begin{aligned}
&\sum_l \mathrm{e}^{-\mathrm{i}\boldsymbol{K}\cdot\vec{\tau}_l} \begin{pmatrix} (\tau_l^x)^3 & (\tau_l^x)^2\tau_l^y & \tau_l^x(\tau_l^y)^2 & (\tau_l^y)^3 \end{pmatrix} \\
&\quad = \frac{\omega^{-1}}{8} a^3 \begin{pmatrix} +\mathrm{i}\sqrt{3} & +\dfrac{1}{\sqrt{3}} & +\dfrac{\mathrm{i}}{\sqrt{3}} & +\sqrt{3} \end{pmatrix}, \\
&\sum_l \mathrm{e}^{-\mathrm{i}\boldsymbol{K}'\cdot\vec{\tau}_l} \begin{pmatrix} (\tau_l^x)^3 & (\tau_l^x)^2\tau_l^y & \tau_l^x(\tau_l^y)^2 & (\tau_l^y)^3 \end{pmatrix} \\
&\quad = \frac{1}{8} a^3 \begin{pmatrix} -\mathrm{i}\sqrt{3} & +\dfrac{1}{\sqrt{3}} & -\dfrac{\mathrm{i}}{\sqrt{3}} & +\sqrt{3} \end{pmatrix}.
\end{aligned} \quad (3.6)$$

Then, the slowly-varying nature of the envelope functions leads to

$$\begin{aligned}
&\varepsilon F_{A\uparrow}^K(\boldsymbol{r}) = \gamma(\hat{k}_x - \mathrm{i}\hat{k}_y) F_{B\uparrow}^K(\boldsymbol{r}) \\
&- \frac{\mathrm{i}\delta\gamma'}{4R}\sin\theta(\boldsymbol{r}) F_{B\uparrow}^K(\boldsymbol{r}) + \Big(\frac{\mathrm{i}\delta\gamma'}{4R}\cos\theta(\boldsymbol{r}) + \frac{2\mathrm{i}\delta\gamma p}{R}\Big) F_{B\downarrow}^K(\boldsymbol{r}), \\
&\varepsilon F_{A\uparrow}^{K'}(\boldsymbol{r}) = \gamma(\hat{k}_x + \mathrm{i}\hat{k}_y) F_{B\uparrow}^{K'}(\boldsymbol{r}) \\
&+ \frac{\mathrm{i}\delta\gamma'}{4R}\sin\theta(\boldsymbol{r}) F_{B\uparrow}^K(\boldsymbol{r}) - \Big(\frac{\mathrm{i}\delta\gamma'}{4R}\cos\theta(\boldsymbol{r}) - \frac{2\mathrm{i}\delta\gamma p}{R}\Big) F_{B\downarrow}^K(\boldsymbol{r}),
\end{aligned} \quad (3.7)$$

with $\hat{k}_x = \partial/\mathrm{i}\partial x$, $\hat{k}_y = \partial/\mathrm{i}\partial y$, and

$$\begin{aligned}
\gamma &= -\frac{\sqrt{3}}{2} V_{pp}^{\pi} a, \\
\gamma' &= \frac{\sqrt{3}}{2}(V_{pp}^{\sigma} - V_{pp}^{\pi}) a, \\
p &= 1 - \frac{3}{8}\frac{\gamma'}{\gamma},
\end{aligned} \quad (3.8)$$

where $\boldsymbol{R}$ describing discrete lattice points has been replaced by continuous coordinate $\boldsymbol{r} = (x, y)$. A similar equation can be obtained for a down spin and we have

$$\begin{aligned}
&\varepsilon F_A^K(\boldsymbol{r}) = \gamma(\hat{k}_x - \mathrm{i}\hat{k}_y) F_B^K(\boldsymbol{r}) \\
&+ \Big(\frac{\mathrm{i}\delta\gamma'}{4R}\big[\sigma_X\cos\theta(\boldsymbol{r}) - \sigma_Z\sin\theta(\boldsymbol{r})\big] - \frac{2\delta\gamma p}{R}\sigma_y\Big) F_B^K(\boldsymbol{r}), \\
&\varepsilon F_A^{K'}(\boldsymbol{r}) = \gamma(\hat{k}_x + \mathrm{i}\hat{k}_y) F_B^{K'}(\boldsymbol{r}) \\
&- \Big(\frac{\mathrm{i}\delta\gamma'}{4R}\big[\sigma_X\cos\theta(\boldsymbol{r}) - \sigma_Z\sin\theta(\boldsymbol{r})\big] + \frac{2\delta\gamma p}{R}\sigma_y\Big) F_B^{K'}(\boldsymbol{r}),
\end{aligned} \quad (3.9)$$

where

$$F_A^K(\boldsymbol{r}) = \begin{pmatrix} F_{A\uparrow}^K(\boldsymbol{r}) \\ F_{A\downarrow}^K(\boldsymbol{r}) \end{pmatrix}, \quad F_B^K(\boldsymbol{r}) = \begin{pmatrix} F_{B\uparrow}^K(\boldsymbol{r}) \\ F_{B\downarrow}^K(\boldsymbol{r}) \end{pmatrix}, \quad (3.10)$$

and

$$F_A^{K'}(\boldsymbol{r}) = \begin{pmatrix} F_{A\uparrow}^{K'}(\boldsymbol{r}) \\ F_{A\downarrow}^{K'}(\boldsymbol{r}) \end{pmatrix}, \quad F_B^{K'}(\boldsymbol{r}) = \begin{pmatrix} F_{B\uparrow}^{K'}(\boldsymbol{r}) \\ F_{B\downarrow}^{K'}(\boldsymbol{r}) \end{pmatrix}. \quad (3.11)$$

With the use of

$$\sigma_x(\boldsymbol{r}) = \sigma_X\cos\theta(\boldsymbol{r}) - \sigma_Z\sin\theta(\boldsymbol{r}), \quad (3.12)$$

these can be rewritten as

$$\begin{aligned}\varepsilon F_A^K(\boldsymbol{r}) &= \gamma(\hat{k}_x - \mathrm{i}\hat{k}_y)F_B^K(\boldsymbol{r}) \\ &\quad + \Big(\frac{\mathrm{i}\delta\gamma'}{4R}\sigma_x(\boldsymbol{r}) - \frac{2\delta\gamma p}{R}\sigma_y\Big)F_B^K(\boldsymbol{r}), \\ \varepsilon F_A^{K'}(\boldsymbol{r}) &= \gamma(\hat{k}_x + \mathrm{i}\hat{k}_y)F_B^{K'}(\boldsymbol{r}) \\ &\quad - \Big(\frac{\mathrm{i}\delta\gamma'}{4R}\sigma_x(\boldsymbol{r}) + \frac{2\delta\gamma p}{R}\sigma_y\Big)F_B^{K'}(\boldsymbol{r}).\end{aligned} \tag{3.13}$$

Similar equations can be obtained for envelopes F_B^K and $F_B^{K'}$ and the resulting effective-mass equation is written as

$$\mathcal{H}\boldsymbol{F}^K(\boldsymbol{r}) = \varepsilon\boldsymbol{F}^K(\boldsymbol{r}), \quad \mathcal{H}'\boldsymbol{F}^{K'}(\boldsymbol{r}) = \varepsilon\boldsymbol{F}^{K'}(\boldsymbol{r}), \tag{3.14}$$

where the matrix-Hamiltonian is written as

$$\mathcal{H} = \begin{pmatrix} 0 & \gamma(\hat{k}_x - \mathrm{i}\hat{k}_y) + \dfrac{\mathrm{i}\delta\gamma'}{4R}\sigma_x(\boldsymbol{r}) - \dfrac{2\delta\gamma p}{R}\sigma_y \\ \gamma(\hat{k}_x + \mathrm{i}\hat{k}_y) - \dfrac{\mathrm{i}\delta\gamma'}{4R}\sigma_x(\boldsymbol{r}) - \dfrac{2\delta\gamma p}{R}\sigma_y & 0 \end{pmatrix}, \tag{3.15}$$

for the K point and

$$\mathcal{H}' = \begin{pmatrix} 0 & \gamma(\hat{k}_x + \mathrm{i}\hat{k}_y) - \dfrac{\mathrm{i}\delta\gamma'}{4R}\sigma_x(\boldsymbol{r}) - \dfrac{2\delta\gamma p}{R}\sigma_y \\ \gamma(\hat{k}_x - \mathrm{i}\hat{k}_y) + \dfrac{\mathrm{i}\delta\gamma'}{4R}\sigma_x(\boldsymbol{r}) - \dfrac{2\delta\gamma p}{R}\sigma_y & 0 \end{pmatrix}, \tag{3.16}$$

for the K' point.

This effective-mass equation has been derived based on a simple tight-binding model with a single p_z orbital at each carbon atom. In the tight-binding model, the realistic values of the parameters are $V_\pi \sim -3$ eV and $V_\sigma \sim 5$ eV, i.e., $\gamma_0 = -V_\pi \sim 3$ eV and $\gamma_1 = V_\sigma - V_\pi \sim 8$ eV, which gives $\gamma'/\gamma \sim 8/3$ and $|p| \lesssim 0.1$. However, the effective-mass equation itself is likely to be much more general if δ and p as well as γ and γ' are regarded as parameters to be determined experimentally rather than given by eqs. (2.7) and (3.8).

§4. Energy Levels and Spin Scattering

In the absence of the spin-orbit interaction, i.e., $\delta = 0$, the energy levels with wave vector k in the axis direction in the vicinity of the K point is given as

$$\varepsilon_{\nu\varphi}^s(n,k) = s\gamma\sqrt{\kappa_{\nu\varphi}(n)^2 + k}, \tag{4.1}$$

with

$$\kappa_{\nu\varphi}(n) = \frac{2\pi}{L}\Big(n + \varphi - \frac{\nu}{3}\Big), \tag{4.2}$$

where $L = |\boldsymbol{L}|$, n is an integer, $\nu = 0$ and ± 1 for a metallic and semiconducting CN, respectively, $\varphi = \phi/\phi_0$ is a magnetic flux passing through the CN cross section measured in units of the flux quantum $\phi_0 = ch/e$, and $s = +1$ and -1 for conduction and valence bands, respectively. The corresponding wave functions are written as

$$\boldsymbol{F}_{snk}^K(\boldsymbol{r}) = \boldsymbol{F}_{snk}^K\frac{1}{\sqrt{AL}}\exp[\mathrm{i}\kappa_{\nu\varphi}(n)x + \mathrm{i}ky], \tag{4.3}$$

with

$$\boldsymbol{F}_{snk}^K = \frac{1}{\sqrt{2}}\begin{pmatrix} b_{\nu\varphi}(n,k) \\ s \end{pmatrix}, \tag{4.4}$$

and

$$b_{\nu\varphi}(n,k) = \frac{\kappa_{\nu\varphi}(n) - \mathrm{i}k}{\sqrt{\kappa_{\nu\varphi}(n)^2 + k^2}}, \tag{4.5}$$

where A is the length of the nanotube.

The spin-orbit term proportional to $\sigma_x(\boldsymbol{r})$ varies spatially like $\exp(+2\pi\mathrm{i}x/L)$ or $\exp(-2\pi\mathrm{i}x/L)$ as a function of x in the circumference direction and its expectation value for states with same n vanishes. Therefore, its effect can be neglected to the lowest order. When this term is ignored completely, the motion for an electron with $\sigma = +1$ and that for $\sigma = -1$ are completely decoupled, where $\sigma = +1$ is the state with spin in the positive y direction parallel to the axis and $\sigma = -1$ that in the negative y direction. The spin-orbit term corresponds to a change of $\hat{k}_x$ into $\hat{k}_x - (2\delta\gamma p/R)\sigma$, which is equivalent to the presence of an Aharonov-Bohm magnetic flux $\phi_{\mathrm{so}} = -2\delta\sigma p\phi_0$ passing through the CN cross section. The energy levels can be obtained by replacing $\kappa_{\nu\varphi}(n)$ by $\kappa_{\nu\varphi\sigma}(n)$ with

$$\kappa_{\nu\varphi\sigma}(n) = \frac{2\pi}{L}\Big(n + \varphi - \frac{\nu}{3} - 2\delta p\sigma\Big). \tag{4.6}$$

For a metallic nanotube ($\nu = 0$) in the absence of a magnetic flux ($\varphi = 0$), a small energy gap given by $\varepsilon_G^{\mathrm{so}} = 8\pi\delta\gamma|p|/L$ opens up but no spin-splitting is present for the band $n = 0$. This gap gives rise to a weak backward scattering even by a slowly-varying potential in contrast to the case in the absence of a spin-orbit interaction.[21,22] In other cases, the spin-orbit term gives rise to a small spin splitting because $|\kappa_{\nu\phi\sigma}(n)|$ depends on the spin σ. The fact that the Hamiltonian is separable into that with $\sigma = +1$ and -1 shows that there is no spin scattering for scatterers having spin-independent potential. In fact, an electron with spin $\sigma = +1$ cannot be scattered into a state with spin $\sigma = -1$ and vice versa. On the other hand, a spin having its component perpendicular to the axis undergoes a precession due to the "effective magnetic field" in the axis direction.

Spin scattering can be induced if the term proportional to $\sigma_x(\boldsymbol{r})$ is included. In the representation where σ_y is diagonalized,

$$\sigma_x(\boldsymbol{r}) = \begin{pmatrix} 0 & \exp(-2\pi\mathrm{i}x/L) \\ \exp(+2\pi\mathrm{i}x/L) & 0 \end{pmatrix}. \tag{4.7}$$

Therefore, the lowest order perturbation theory gives

$$\begin{aligned}\boldsymbol{F}_{snk\uparrow}^K(\boldsymbol{r}) &= \boldsymbol{F}_{snk}^K(\boldsymbol{r})\chi_\uparrow + \sum_{s'}\boldsymbol{F}_{s'n+1k}^K(\boldsymbol{r})\chi_\downarrow \\ &\quad \times \frac{-\mathrm{i}\delta\gamma'}{8R}\frac{s'b_{\nu\varphi}(n,k) - sb_{\nu\varphi}(n+1,k)^*}{\varepsilon_{\nu\varphi}^s(n,k) - \varepsilon_{\nu\varphi}^{s'}(n+1,k)},\end{aligned} \tag{4.8}$$

and

$$\begin{aligned}\boldsymbol{F}_{snk\downarrow}^K(\boldsymbol{r}) &= \boldsymbol{F}_{snk}^K(\boldsymbol{r})\chi_\downarrow + \sum_{s'}\boldsymbol{F}_{s'n-1k}^K(\boldsymbol{r})\chi_\uparrow \\ &\quad \times \frac{-\mathrm{i}\delta\gamma'}{8R}\frac{s'b_{\nu\varphi}(n,k) - sb_{\nu\varphi}(n-1,k)^*}{\varepsilon_{\nu\varphi}^s(n,k) - \varepsilon_{\nu\varphi}^{s'}(n-1,k)},\end{aligned} \tag{4.9}$$

where $\chi_\uparrow$ and $\chi_\downarrow$ are the spinor functions for $\sigma = 1$ and -1, respectively, and a small corrections in the energy denominator due to the spin-orbit term proportional to σ_y have been completely neglected. This mixing between different bands again leads to a weak backward scattering even by a slowly-varying potential. In fact, the matrix element for scattering from $k_+ = +k$ with $\sigma = +1$ to

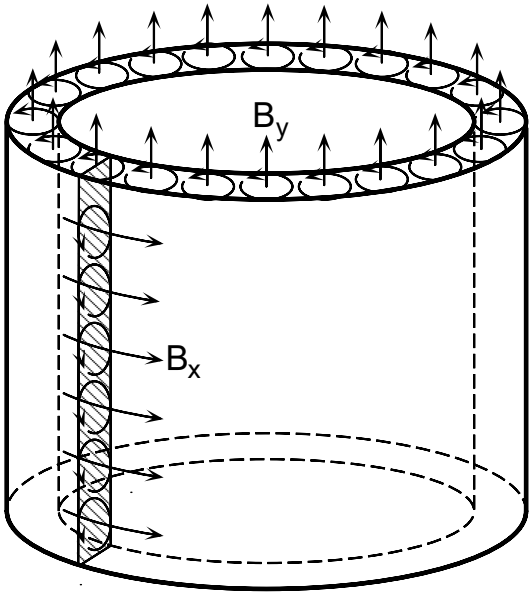

Fig. 4 A schematic illustration of effective magnetic fields for the electron spin induced by a spin-orbit interaction. A circular current induced at each carbon atom leads to nonvanishing angular momenta $\langle l_x\rangle \propto B_x$ and $\langle l_y\rangle \propto B_y$ in the circumference and axis directions.

$k_- = -k$ with $\sigma = -1$ in the band $n = 0$ in the metallic case in the absence of a magnetic flux is calculated as $V(2\pi/L, 2k)(-\mathrm{i}\delta\gamma'/2\gamma)$ for $k \ll 2\pi/L$, with

$$V(2\pi/L, 2k) = \int \frac{\mathrm{d}x\mathrm{d}y}{AL} V(\boldsymbol{r}) \exp\Big(\frac{2\pi \mathrm{i}x}{L} + 2\mathrm{i}ky\Big), \quad (4.10)$$

where $V(\boldsymbol{r})$ is the impurity potential. This backward scattering gives rise to a small spin relaxation. A similar spin relaxation process is possible for short-range scatterers, which induces backward scattering even in the absence of a spin-orbit interaction.

Quite recently, a spin-dependent conductance was measured in nanotubes and a lower bound of the spin diffusion length was estimated to be ~ 2500 Å.[28] The present theory shows that this small diffusion length may be explained by the spin-orbit interaction. The actual estimation is difficult in the absence of the information on the nature of scatterers in experimental samples.

§5. Discussion

In an isotropic atom, the spin-orbit interaction is usually written as $\mathcal{H}_{\mathrm{so}} = \lambda(\boldsymbol{l}\cdot\boldsymbol{s})$, where $\boldsymbol{l}$ is the orbital angular momentum and $\boldsymbol{s} = \vec{\sigma}/2$ is the spin angular momentum. Because of a nonzero curvature and thickness of the nanotube, a circular current is induced around each carbon atom in the circumference ($\langle l_x\rangle \propto B_x$) and axis ($\langle l_y\rangle \propto B_y$) direction as schematically illustrated in Fig. 4, where B_x and B_y are effective magnetic fields. Such circular currents should vanish for states at the Γ point of a 2D graphite due to symmetry, but can be nonzero for states at K and K' points away from the Γ point. This is likely to be the origin of the term proportional to σ_x and σ_y in the effective Hamiltonian, although situations are actually more complicated because such terms appear in off-diagonal elements. The spin-orbit term in the $\boldsymbol{k}\cdot\boldsymbol{p}$ Hamiltonian vanishes in the limit of $a/R \to 0$, i.e., in the limit of 2D graphite, and therefore is different from those discussed previously for bulk graphite.[29]

The parameter $\delta = \Delta/3\varepsilon_{\pi\sigma}$ describing the strength of the spin-orbit interaction should be determined by experiments because its exact estimation is quite difficult. This is because the spin-orbit parameter Δ is not known in graphite and because the simple tight-binding model used in the present paper is not so accurate and can describe the band structure only qualitatively. In fact, in simple tight-binding models $\varepsilon_{\pi\sigma}$ is usually neglected completely.

Nevertheless, we may be able to provide a very rough estimation of δ as follows: We first assume that Δ is not much different between graphite and diamond and use $\Delta \approx 6$ meV obtained in diamond.[30] Next $\varepsilon_{\pi\sigma}$ is assumed to be of the order of a few electron volts smaller than the difference between the π bands and σ bands in 2D graphite, of the order of ~ 10 eV.[31] Then, we have $10^{-3} \lesssim \delta \lesssim 10^{-2}$. Note, however, that this estimation is too sensitive to that of $\varepsilon_{\pi\sigma}$ and is likely to be quite inappropriate.

So far, we have neglected terms of the order of $(a/R)^2$ completely. Largest effects arise from the correction given by eq. (2.28). Its effect can be calculated in a similar manner and leads to a term corresponding to the replacement

$$\begin{aligned}
\hat{k}_x - \mathrm{i}\hat{k}_y &\to \hat{k}_x - \mathrm{i}\hat{k}_y \pm \frac{\gamma a}{4\sqrt{3}R^2}\Big[\Big(1 - \frac{\gamma'}{2\gamma}\Big)\mathrm{e}^{+3\mathrm{i}\eta} + \frac{\gamma'}{8\gamma}\mathrm{e}^{-3\mathrm{i}\eta}\Big], \\
\hat{k}_x + \mathrm{i}\hat{k}_y &\to \hat{k}_x + \mathrm{i}\hat{k}_y \pm \frac{\gamma a}{4\sqrt{3}R^2}\Big[\Big(1 - \frac{\gamma'}{2\gamma}\Big)\mathrm{e}^{-3\mathrm{i}\eta} + \frac{\gamma'}{8\gamma}\mathrm{e}^{+3\mathrm{i}\eta}\Big],
\end{aligned} \quad (5.1)$$

in the effective Hamiltonian given by eqs. (3.15) and (3.16), where the upper sign corresponds to the K point and the lower sign to the K' point. The extra term causes a shift in the origin of $\hat{k}_x$ and $\hat{k}_y$ by Δk_x and Δk_y, respectively, where

$$\begin{aligned}
\Delta k_x &= \mp\frac{a}{4\sqrt{3}R^2}\Big(1 - \frac{3}{8}\frac{\gamma'}{\gamma}\Big)\cos 3\eta, \\
\Delta k_y &= \mp\frac{a}{4\sqrt{3}R^2}\Big(\frac{5}{8}\frac{\gamma'}{\gamma} - 1\Big)\sin 3\eta.
\end{aligned} \quad (5.2)$$

The shift Δk_x leads to an opening of a small band gap for nanotubes with a small diameter except in the armchair case ($\eta = \pi/6$). This gap is expected to be very small because $\gamma'/\gamma \sim 8/3$ as mentioned in a previous section. In armchair nanotubes, Δk_y gives rise to a shift of the wave vector corresponding to $\varepsilon = 0$, for example, from $k = 2\pi/3a$ to $k = (2\pi/3a) + \Delta k$ with $\Delta k = -a/4\sqrt{3}R^2[(5/8)(\gamma'/\gamma) - 1]$. The wave vector is shifted to the direction of the Γ point for $\gamma'/\gamma \sim 8/3$.

Several first-principles calculations were reported on the band structure of nanotubes, which seems to show that the shift is quite sensitive to details of methods. In fact, Hamada et al[4] gave $\Delta k < 0$ for $(n_a, n_b) = (12, 6)$ (so-called (6,6) armchair nanotube) and Mintmire et al[5] gave $\Delta k > 0$ for $(n_a, n_b) = (10, 5)$ (so-called (5,5) tube). Actually, mixing between π and σ orbitals should also be considered when we discuss curvature effects of the order $(a/R)^2$. Results of Δk_x and Δk_y which can be obtained by putting $\gamma' = 0$ in eq. (5.2) were derived,[32] but effects

of more important V_{pp}^{σ} were completely neglected in this calculation.

§6. Summary and Conclusion

An effective-mass Hamiltonian has been derived for carbon nanotubes in the presence of a weak spin-orbit interaction. The spin-orbit interaction introduces terms corresponding to effective magnetic fields in the circumference and axis directions giving rise to a kind of a spin-Zeeman energy. Because of such terms scatterers with a long-range potential induce a weak backward scattering in metallic nanotubes in which they do not cause any backscattering in the absence of a spin-orbit interaction. As each energy becomes no longer a spin eigen-state, such impurity scattering causes spin relaxation.

Acknowledgments

This work was supported in part by Grants-in-Aid for Scientific Research and for Priority Area, Fullerene Network, from Ministry of Education, Science and Culture.

1) S. Iijima: Nature (London) **354** (1991) 56.
2) S. Iijima and T. Ichihashi: Nature (London) **363** (1993) 603.
3) D. S. Bethune, C. H. Kiang, M. S. de Vries, G. Gorman, R. Savoy, J. Vazquez and R. Beyers: Nature (London) **363** (1993) 605.
4) N. Hamada, S. Sawada and A. Oshiyama: Phys. Rev. Lett. **68** (1992) 1579.
5) J. W. Mintmire, B. I. Dunlap and C. T. White: Phys. Rev. Lett. **68** (1992) 631.
6) R. Saito, M. Fujita, G. Dresselhaus and M. S. Dresselhaus: Phys. Rev. B **46** (1992) 1804; Appl. Phys. Lett. **60** (1992) 2204.
7) M. S. Dresselhaus, G. Dresselhaus and R. Saito: Phys. Rev. B **45** (1992) 6234.
8) R. A. Jishi, M. S. Dresselhaus and G. Dresselhaus: Phys. Rev. B **47** (1993) 16671.
9) K. Tanaka, K. Okahara, M. Okada and T. Yamabe: Chem. Phys. Lett. **191** (1992) 469.
10) Y. D. Gao and W. C. Herndon: Mol. Phys. **77** (1992) 585.
11) D. H. Robertson, D. W. Berenner and J. W. Mintmire: Phys. Rev. B **45** (1992) 12592.
12) C. T. White, D. C. Robertson and J. W. Mintmire: Phys. Rev. B **47** (1993) 5485.
13) H. Ajiki and T. Ando: J. Phys. Soc. Jpn. **62** (1993) 1255.
14) H. Ajiki and T. Ando: J. Phys. Soc. Jpn. **65** (1996) 505.
15) H. Ajiki and T. Ando: J. Phys. Soc. Jpn. **62** (1993) 2470; *ibid* **64** (1995) 4382.
16) H. Ajiki and T. Ando: Physica B **201** (1994) 349; Jpn. J. Appl. Phys. Suppl. **34** (1995) 107.
17) T. Ando: J. Phys. Soc. Jpn. **66** (1997) 1066.
18) N. A. Viet, H. Ajiki and T. Ando: J. Phys. Soc. Jpn. **63** (1994) 3036.
19) H. Ajiki and T. Ando: J. Phys. Soc. Jpn. **64** (1995) 260.
20) H. Ajiki and T. Ando: J. Phys. Soc. Jpn. **65** (1996) 2976.
21) T. Ando and T. Nakanishi: J. Phys. Soc. Jpn. **67** (1998) 1704.
22) T. Ando, T. Nakanishi and R. Saito: J. Phys. Soc. Jpn. **67** (1998) 2857.
23) T. Ando, T. Nakanishi and M. Igami: J. Phys. Soc. Jpn. **68**, No. 12 (1999).
24) H. Suzuura and T. Ando: Mol. Cryst. Liq. Cryst. (in press).
25) H. Matsumura and T. Ando: J. Phys. Soc. Jpn. **67** (1998) 3542.
26) R. Tamura and M. Tsukada: Phys. Rev. B **58** (1998) 8120.
27) H. Matsumura and T. Ando: Mol. Cryst. Liq. Cryst. (in press).
28) K. Tsukagoshi, B. W. Alphenaar and H. Ago: Nature **401** (1999) 572.
29) G. Dresselhaus and M.S. Dresselhaus: Phys. Rev. **140** (1965) A401.
30) C. J. Rauch: *Proc. Int. Conf. Phys. Semiconductors* (The Institute of Physics, London, 1962), p. 276.
31) G. S. Painter and D. E. Ellis: Phys. Rev. B **1** (1970) 4747.
32) C. L. Kane and E. J. Mele: Phys. Rev. Lett. **78** (1997) 1932.